HHS Public Access

Author manuscript

Phys Med Biol. Author manuscript; available in PMC 2017 September 28.

Published in final edited form as:

Phys Med Biol. ; 62(15): 6144–6163. doi:10.1088/1361-6560/aa77df.

Combined passive acoustic mapping and magnetic resonance thermometry for monitoring phase-shift nanoemulsion enhanced focused ultrasound therapy

Calum Crake[1], **F. Can Meral**[1], **Mark T. Burgess**[2], **Iason T. Papademetriou**[2], **Nathan J. McDannold**[1], and **Tyrone M. Porter**[2,3,*]

[1]Department of Radiology, Brigham and Women's Hospital, Harvard Medical School, 221 Longwood Avenue, Boston, MA 02115, USA

[2]Department of Mechanical Engineering, Boston University, Boston, MA 02215, USA

[3]Department of Biomedical Engineering, Boston University, Boston, MA 02215, USA

Abstract

Focused ultrasound (FUS) has the potential to enable precise, image-guided noninvasive surgery for the treatment of cancer in which tumors are identified and destroyed in a single integrated procedure. However, success of the method in highly vascular organs has been limited due to heat losses to perfusion, requiring development of techniques to locally enhance energy absorption and heating. In addition, FUS procedures are conventionally monitored using MRI, which provides excellent anatomical images and can map temperature, but is not capable of capturing the full gamut of available data such as the acoustic emissions generated during this inherently acoustically-driven procedure. Here, we employed phase-shift nanoemulsions (PSNE) embedded in tissue phantoms to promote cavitation and hence temperature rise induced by FUS. In addition, we incorporated passive acoustic mapping (PAM) alongside simultaneous MR thermometry in order to visualize both acoustic emissions and temperature rise, within the bore of a full scale clinical MRI scanner. Focal cavitation of PSNE could be resolved using PAM and resulted in accelerated heating and increased the maximum elevated temperature measured via MR thermometry compared to experiments without nanoemulsions. Over time, the simultaneously acquired acoustic and temperature maps show translation of the focus of activity towards the FUS transducer, and the magnitude of the increase in cavitation and focal shift both increased with nanoemulsion concentration. PAM results were well correlated with MRI thermometry and demonstrated greater sensitivity, with ability to detect cavitation before enhanced heating was observed. The results suggest that PSNE could be beneficial for enhancement of thermal focused ultrasound therapies and that PAM could be a critical tool for monitoring of this process.

Keywords

passive acoustic mapping; magnetic resonance imaging; thermal ablation; phase-shift nanoemulsion; cavitation; beamforming; focused ultrasound

*Corresponding author: Tyrone Porter (tmp@bu.edu).

1. Introduction

Focused ultrasound (FUS) surgery utilizes high intensity focused ultrasound (HIFU) for the noninvasive ablation of tissues deep within the body such as benign or malignant tumors (Kennedy 2005, Jolesz 2009). The technique has been used in the treatment of uterine fibroids (Tempany *et al* 2003, Stewart *et al* 2003), tumors in the breast (Hynynen *et al* 2001), pancreas (Wang and Sun 2002, Wu *et al* 2005), liver (ter Haar *et al* 1989, Illing *et al* 2005, Leslie *et al* 2008), prostate (Thüroff *et al* 2003), bone (Catane *et al* 2007), and kidney (Illing *et al* 2005). Although FUS ablation in highly vascular organs such as the kidney has been demonstrated, the well perfused nature of the organ may limit the delivered thermal dose due to the heat loss by perfusion. This may risk incomplete treatment, requiring extended treatment times or high acoustic power levels in order to ablate the entire tumor volume while maintaining acceptable pre- and post-focal heating in the beam path (Chen *et al* 1993, Illing *et al* 2005). In order to improve the scope of FUS to include challenging targets such as the kidney new techniques are required to locally increase energy absorption, accelerate heating, and improve efficacy.

Ultrasound contrast agents (UCA) are micron sized gas bubbles enclosed in a biocompatible shell. These agents are clinically approved and currently used in routine medical ultrasound imaging for applications such as left ventricle visualization in the heart or focal lesion detection in the liver (Albrecht *et al* 2004, Claudon *et al* 2012). At higher ultrasound powers, acoustic cavitation of bubbles is known to improve the effects of FUS treatment by enhancing heat deposition through mechanisms such as multiple scattering, increased absorption and broadband acoustic emissions from inertial collapse (Coussios *et al* 2007, Holt and Roy 2001). Such use of UCA to enhance thermal effects of FUS has been investigated in various *in vitro* (Tung *et al* 2006) and *in vivo* studies (Tran *et al* 2003, Yu *et al* 2003, McDannold *et al* 2006). Alternatively, it is possible to use high pressure pulses to create bubbles from nuclei within the tissue itself (Lele 1987, Hynynen 1991), however the pressure amplitudes required can be several megapascals and vary significantly between different types of tissue (Gateau *et al* 2011a). Additionally, the heterogeneous nature of tissue and particularly tumors (Heppner and Miller 1983) makes bubble formation difficult to control (Sokka *et al* 2003). FUS ablations with UCA can reduce the pressure threshold for cavitation and hence heating enhancement; however, current UCA introduce their own limitations. First, microbubbles are too large to extravasate from blood vessels so are confined to the vasculature. This means that treatment which requires interaction with the microbubbles themselves can only make use of the concentration of microbubbles currently circulating, and cannot allow local extravascular accumulation in the desired location. The use of nanometer sized agents, which can extravasate into tissue as a result of their small size and accumulate in tumors would thus be advantageous for enhancement of FUS treatment. Second, UCA have a relatively short circulation time (on the order of minutes), which puts an upper limit on the duration of treatment, and thus size of region that may be treated. Agents that circulate for longer periods could thus allow longer treatment times. If the agents are appropriately sized they could also accumulate in the desired region, allowing greater impact on therapy.

Phase-shift nanoemulsions (PSNE) are nanometer size agents (100–300nm) with a lipid shell containing a liquid perfluorocarbon (PFC) core (Zhang and Porter 2010, Dayton *et al* 2006, Kripfgans *et al* 2000, Reznik *et al* 2012). The liquid PFC enclosed in the PSNE can be vaporized by temperature elevation or application of a high amplitude rarefactional pressure (~5MPa), i.e. acoustic droplet vaporization (Kripfgans *et al* 2000, 2004, Zhang *et al* 2011). Once vaporized PSNE will rapidly grow into micron-scale gas bubbles which can be used as cavitation nuclei for enhanced heating (Zhang and Porter 2010, Zhang *et al* 2011, 2013). Particles which are smaller than 500nm in size are likely to accumulate in tumors due to the leaky vasculature and underdeveloped lymphatic drainage of tumors, a phenomenon known as the enhanced permeability and retention (EPR) effect (Ishida *et al* 1999, Maeda *et al* 2000, Yuan *et al* 1995). PSNE can accumulate in tumors due to EPR effect and may then be vaporized to seed bubbles inside the region to be ablated (Kopechek *et al* 2013). To promote acoustic vaporization of PSNE composite acoustic pulses can be used in which a short high-amplitude pulse is used first for vaporizing the PSNE, followed by a longer lower-amplitude burst to promote cavitation-enhanced heating.

Guidance and monitoring of noninvasive treatment modalities such as HIFU with medical imaging is essential. For FUS the gold standard for targeting, planning and monitoring is currently magnetic resonance imaging (MRI) (Chung *et al* 1996, Jolesz 2009), as this provides excellent anatomical images and can also be used for thermal monitoring of ablative therapies. The most common form of MR thermometry currently in clinical use utilizes the shift in proton resonance frequency with temperature to convert phase-sensitive MR images into temperature maps (Ishihara *et al* 1995). MR thermometry has been used together with FUS for monitoring and controlling treatment (Jolesz 2009, Quesson *et al* 2000, Palussière *et al* 2003, Mougenot *et al* 2004), including during clinical studies (Tempany *et al* 2003, Elias *et al* 2016). MRI-guided FUS has been approved by the FDA for applications including treatment of uterine fibroids and noninvasive brain surgery to treat essential tremor (U.S. Food and Drug Administration, 2004, 2016).

Alternatively, ultrasound imaging can be used for guidance and monitoring (Yang *et al* 1992, Wu *et al* 2004) of FUS. Use of ultrasound imaging in place of MRI for guidance and monitoring would be beneficial as the acoustic emissions during treatment can provide additional information which could not be detected with MRI. Use of sonography in place of MRI could also make FUS therapy accessible to larger populations by significantly reducing the cost. However monitoring using conventional (B-mode) ultrasound imaging may be difficult during the application of HIFU due to interference from the therapeutic ultrasound. In addition, the echogenicity of the lesions formed during FUS ablations is frequently insufficient for reliable detection using conventional imaging methods (Jensen et al 2012).

Alternatively, ultrasonic detectors can be used passively – i.e. without signals being transmitted as in conventional imaging – to monitor FUS treatments (Coussios *et al* 2007, Sokka *et al* 2003). Specifically in the presence of cavitation nuclei the amount of cavitation being detected can be correlated with the amount of heat being deposited (Farny 2007, Farny *et al* 2009). By utilizing an array of transducers as passive detectors it becomes possible to spatially resolve the location of cavitation activity. Such passive acoustic mapping (PAM) makes use of time (Gyongy and Coussios 2010, Gateau *et al* 2011b) or frequency-domain

(Salgaonkar *et al* 2009, Arvanitis *et al* 2016, Haworth *et al* 2012) beamforming methods to reconstruct the distribution of acoustic sources such as cavitating microbubbles (O'Reilly *et al* 2014, Deng *et al* 2016, Choi and Coussios 2012). PAM has been utilized for various FUS applications including monitoring of ablation in tissue (Jensen *et al* 2012), microbubble activity in the brain (Arvanitis *et al* 2013, Vignon *et al* 2013), transfection of cells (Lee *et al* 2015, Myers *et al* 2016) and investigation of microbubble targeting (Crake *et al* 2015). As PAM provides information on the spatial distribution and intensity of cavitation activity this could be beneficial for monitoring of PSNE-enhanced ablation by enabling prediction and control of cavitation-enhanced heating.

In this paper we demonstrated the use of passive acoustic mapping alongside MRI thermometry for monitoring vaporization, cavitation and heating enhanced by PSNE-embedded hydrogels within the bore of a clinical MRI scanner.

2. Methods

2.1. Phase-shift nano-emulsion preparation

Phospholipid coated phase-shift nanoemulsions (PSNE) were prepared using an emulsification and extrusion procedure (Kopechek *et al* 2012, Burgess and Porter 2015). The lipids dipalmitoylphosphocholine (DPPC) and dipalmitoylphosphoethanolamine-polyethylene glycol (DPPE-PEG2000) (Avanti Polar Lipids, Alabaster, AL, USA) were weighed into a glass vial and dissolved with chloroform (Sigma-Aldrich, St. Louis, MO, USA) at a molar ratio of 95:5 (DPPC:DPPE-PEG2000). The chloroform was evaporated with a stream of argon gas and placed under vacuum overnight. Subsequently, the lipid film was hydrated with phosphate buffered saline (PBS) (Boston BioProducts, Ashland, MA, USA) to a final concentration of 1 mg/mL and placed in a 50°C water bath. Periodic vortexing and bath sonication (Cole-Parmer, Vernon Hills, IL, USA) was performed to ensure complete hydration of the lipid film. High power probe sonication (20% output power; model VC505/500W, Sonic & Materials, Newtown, CT, USA) was performed after hydration for one minute to produce a clear lipid solution.

Dodecafluoropentane (DDFP) (Exfluor Research Corporation, Round Rock, TX, USA) emulsions were formed by adding 100 μL DDFP to 3 mL of the lipid solution, and sonicating with the high power probe tip sonicator. The sample was maintained in an ice water bath and sonicated using a pulsed scheme (25% output power, 10 seconds on, 50 seconds of, one minute total on time) to prevent heating and vaporization of the perfluorocarbon. The resulting emulsion was then diluted with 7 mL of cold PBS prior to extrusion. A pressure extruder (LIPEX, Northern Lipids Inc., Burnaby, British Columbia) was used to pass the emulsion 10 times through two stacked 200 nm polycarbonate filters to form PSNE. Excess lipid was removed by pelleting the PSNE with three centrifugal washes at 3,000 g for 5 minutes. Each time the pellet was resuspended in fresh PBS. The solution was stored at 4°C until use.

Samples of the resulting suspension were analyzed using dynamic light scattering (90Plus, Brookhaven Instruments, Holtsville, NY, USA). In addition, to confirm that no large particles were present and that the PSNE could be vaporized a 100 μL sample of the

suspension was diluted in 1 mL water and observed using an optical microscope (CKX41, Olympus, Japan) before and after sonication with the probe sonicator (25% power, 30s).

2.2. Gel Phantom Preparation

In order to mimic the *in vivo* scenario of accumulated PSNE in tissue, PSNE were dispersed in polyacrylamide gel phantoms (Lafon *et al* 2005, Kopechek *et al* 2012). All chemicals for the gel phantom fabrication were purchased from Sigma-Aldrich (St. Louis, MO, USA) unless noted otherwise. Each gel was ~10 mL in volume and polymerized in 50 mL centrifuge tubes. The recipe for individual gels consisted of 1.75 mL acrylamide/bis-acrylamide (19:1, 40% solution), 1 mL of TRIS buffer (1 M, pH 8), 0.8 g albumin powder dissolved in 7 mL water, 100 μL of 10% w/v ammonium persulfate solution, 100 μL of PSNE solution (i.e. ~1% of gel volume) and 10 μL of TEMED to initiate polymerization. The acrylamide, TRIS, albumin and APS were mixed, heated to 40°C and placed under vacuum for one hour to degas the solution, and then aliquoted into the centrifuge tubes. PSNE were then added at various concentrations (100% = 100μL PSNE stock, 10%= 10μL PSNE, 90μL water etc.) and vortexed gently to disperse throughout the gel, and TEMED added to catalyze polymerization. For control experiments gels were made with an equivalent quantity of PBS in place of PSNE suspension. For experiments using MR thermometry the gels were embedded in a larger gel base made from 3% agar (Hall *et al* 1997) to eliminate motion artifacts which could disrupt the phase-sensitive thermometry sequence.

2.3. FUS Sonication

A schematic of the experimental setup is given in Figure 1. PSNE-containing or control polyacrylamide gels were sonicated using a spherically focused HIFU transducer (constructed in house, diameter 10 cm, f# 0.8) with a center frequency of 1.653 MHz. The beam pattern and output efficiency of the focused transducer were characterized as a function of the driving voltage using a needle hydrophone and force balance (Hynynen 1991). Acoustic emissions from the gels were received with a broadband 128-element linear imaging array (5 MHz center frequency, 58 mm aperture, L558, Acuson, Siemens Medical Solutions USA, Inc., Malvern, PA) positioned such that the focal region was within the imaging plane and FUS propagation was in the transverse direction with respect to the imaging array. This orientation was chosen such that the resolution of the acoustic data was best in the direction of FUS propagation (Gyöngy 2010). Polyacrylamide gels were seated inside an agar base and positioned at the geometric focus of the HIFU transducer with a fixture frame whose position can be adjusted with respect to the transducers. The assembly was immersed in a tank filled with degassed deionized water heated to 37°C and clamped to the patient table of the MRI scanner. A receive-only MRI surface coil (15cm diameter, constructed in house) was placed around the outside of the gel base.

The HIFU transducer was driven by a signal generated using two function generators (33250, Agilent, Santa Clara, CA and 396, Fluke, Everett, WA) in order to generate a two-stage waveform to promote droplet vaporization and cavitation. The signals from the function generators were combined with a power combiner (ZSC-2-2, Mini Circuits, Brooklyn, NY) and amplified with a 50dB power amplifier (240L, E&I, Rochester, NY).

The linear array was connected to an ultrasound research platform (Verasonics Inc., Kirkland, WA). Data acquired using the linear array was stored on a personal computer and processed as described below.

2.4. Passive acoustic mapping

The linear array ultrasound transducer was used for B-mode (active) and passive imaging. In preliminary experiments without MRI, B-mode imaging was used for visualization of the bubble cloud and interspersed with passive imaging. B-mode pulse transmission was disabled for the remaining experiments as the short transmit events were found to produce noise in the MR images. During passive acquisition data was recorded for 110 μs across the 128 channels of the array triggered by the function generator. The process was repeated for each burst resulting in 78 sets of data (‘frames’) per sonication at an average rate of 1.6fps. The passively recorded data from each frame of data were subsequently processed to produce maps of cavitation using the robust Capon beamforming algorithm (Coviello *et al* 2015). The value and position of the peak pixel in the acoustic maps at each time point was used as a measure of the magnitude and location of the acoustic emissions.

2.5. Magnetic resonance imaging

MR guided experiments were performed in a 3 T clinical MRI system (Signa HDxt 3.0T; GE Healthcare, Milwaukee, WI) with sonications as described above. A fast spoiled gradient echo pulse sequence was used to monitor HIFU induced heating. Thirty magnitude and phase images were acquired per sonication at 2.7 second intervals with TE of 13 ms, TR of 19.6 ms, flip angle 30°, bandwidth ±15.6 kHz, 16 cm FOV, 256×128 matrix, and 3 mm slice thickness. MR image acquisition started 3 seconds before the start of sonication in order to acquire two reference phase images, and continued for 25 seconds after sonication to capture cooling, resulting in a total of 28 temperature maps per experiment. The phase images were converted into temperature maps assuming a temperature sensitivity for the proton resonance frequency of 0.01 ppm/°C, equal to that of water (Peters *et al* 1998). The value and position of the peak pixel at each time point was used as a measure of the magnitude and location of heating.

2.6. Experimental protocol

To establish the threshold for detection of PSNE cavitation in this setup, a pressure ramp was conducted using a burst of one million cycles at a pressure ranging from 0 to 5.5 MPa peak negative focal pressure (P^-) in steps of 1.35 MPa. The process was repeated in gels with and without PSNE. We did not separately evaluate the effect of vaporization bursts as this has been studied previously (Zhang and Porter 2010, Zhang *et al* 2013). The amplitude of acoustic emissions was extracted from the PAM data as a measure of cavitation activity. The frequency spectra were also examined as an indication of the type of cavitation activity.

Subsequent sonications made use of a two-step waveform consisting of a 100-cycle burst at 13.7 MPa to promote vaporization, followed by a lower amplitude long tone burst (one million cycles) at 5.5 MPa P^-. The pulsing scheme was repeated 78 times every 640 ms, resulting in a 50 s sonication duration at a duty cycle of 95 %.

To evaluate the effects of PSNE on cavitation and focal heating the PAM and MRI data were examined for three cases: no PSNE (control), low PSNE concentration (5%, intended to result in a 'sub-thermal' degree of cavitation), and high PSNE concentration (20%, intended to result in thermally-relevant cavitation). The value and position of the peak pixels in the thermal and acoustic maps were used as a measure of the magnitude and location of heating and acoustic emissions.

Next, to further explore the effect of PSNE concentration on cavitation and heating the PSNE concentration was varied over six cases (0, 2, 5, 10, 20, 50%). Thermal maps at the time of maximum heating in each case and acoustic maps summed over the duration of each experiment were analyzed by taking the value and location of the peak pixels in the same way as outlined above. Finally, the correlation between these PAM and MRI-derived metrics of cavitation power and heating were explored.

3. Results

3.1. Vaporization of PSNE

DLS measurements indicated the PSNE suspension initially had a mean size of 175.2 ± 2.5 nm and polydispersity index of 0.058 ± 0.023. Microscope images illustrating vaporization of PSNE are shown in Figure 2. Before sonication the majority of individual particles were too small to resolve with conventional optical microscopy due to the diffraction limit – though some scattering of light from the particles could be observed using phase contrast – and the solution appeared clear (Figure 2a). After sonication the emulsion was vaporized into microbubbles and the solution appeared macroscopically cloudy (Figure 2b). This sonication procedure was used before subsequent experiments to confirm PSNE production.

3.2. Cavitation threshold determination

The results of the cavitation threshold experiment are shown in Figure 3. The amplitude of the acoustic emissions was obtained by taking the peak value from each frame of the beamformed data (proportional to source power). As the peak negative focal pressure was increased (Figure 3a) the amplitude of acoustic emissions and number of pulses in which this exceeded that in the control phantom were observed to increase using PSNE. The frequency spectra of the acoustic emissions (Figure 3b) initially showed an increase in harmonics of the driving signal (which suggests vaporization) followed by presence of ultraharmonics and finally increased broadband noise (which suggest non-inertial followed by inertial cavitation). Based on these results, the inertial cavitation threshold for the reported acoustic parameters was estimated to be approximately 5 MPa. To ensure inertial cavitation occurred a value of 5.5 MPa was used for the subsequent experiments.

3.3. B-mode and PAM of PSNE vaporization

Conventional B-mode and passively reconstructed images showing PSNE vaporization are shown in Figure 4. B-mode images taken during treatment (*interspersed* between FUS transducer bursts) showed formation of a bubble cloud at the focus of the FUS transducer within the PSNE-containing phantom (Figure 4a). Passive imaging of the acoustic emissions *during* FUS bursts (Figure 4b) showed that the peak in emissions coincided with the centre

of the observed bubble cloud. B-mode images taken 5s after sonication had ceased (Figure 4c) showed dissolution of the bubble cloud. Note that for this experiment the linear array was rotated 90 degrees (such that FUS propagation is out of the page) to allow easier visualization of the bubble cloud, and that the array was placed closer to the focus than was possible in the experiments using MRI due to the constraints of the MRI coil and gel holder. The PAM image appears elongated in the axial direction of the array due to the point spread function.

3.4. PAM data over time

Passive acoustic maps showing the progression of acoustic emissions over time are shown in Figure 5a, for the cases of no PSNE (control), and low (5%) and high (20%) PSNE concentrations. For display purposes the maps were summed over subsets of the data where the 78 bursts in each experiment were divided into six equal groups of 13 bursts. In control gels without PSNE, low amplitude sporadic activity without a clear center of activity was observed, suggesting absence of significant cavitation. Gels containing 5% diluted PSNE showed focal emissions close to the geometric focus of the FUS transducer, which increased in amplitude during sonication before declining. The energy level summed over the subsets of 13 bursts shown in the figures increased 60-fold compared to that in the control experiment. Finally, in gels containing 20% diluted PSNE cavitation activity was initiated immediately, and proceeded to move towards the FUS transducer over the duration of sonication. The amplitude of emissions was again increased compared to the lower concentration sample.

These results are summarized in Figure 5b, which shows the value and position of the peak in each map for three trials of each of the three conditions. In the control experiments a small signal was present in the very first frame of data (perhaps due to residual gas in the gels) however this immediately fell to a low level background signal close to that obtained from degassed water. As a result in the control experiments, the location of the peak in the maps is not meaningful due to the lack of cavitation activity. The results for experiments including PSNE show similar trends to the individual maps discussed above. In particular, the amplitude of emissions increased between the 5% and 20% PSNE cases. In the 20% PSNE case acoustic emissions were maintained at a level above the control experiments for the entire 50s sonication, and the position of activity gradually shifted towards the FUS transducer over the duration of sonication.

3.5. MRI data over time

MRI thermometry data showing the progression of focal heating over time is shown in Figure 6a for the same 3 conditions as the PAM data above (no PSNE, low and high PSNE concentrations). For display purposes Figure 6a shows every fourth temperature map (7 out of the 28 total per experiment). In the control experiment focal heating was evident above the baseline noise level of the system, and little change in heating was observed using the low concentration of PSNE. However, at the higher PSNE concentration the temperature rise was approximately doubled and location of peak heating appeared to move towards the FUS transducer over time. These results are summarized in Figure 6b, which shows the value and location of the maximum temperature within the MR imaging space over time for three trials

per condition. The maximum temperature increased from 8.8±0.7°C without PSNE to 9.3±2.2°C at 5% diluted PSNE and 19.2±0.8°C at 20% diluted PSNE. Compared to control experiments, the temperature rise from baseline (37°C) was thus approximately doubled using the higher concentration of PSNE. The location of the focus was not consistently resolved above the noise level of the images in the control experiments, however the focus could be located in two out of three of the experiments using 5% diluted PSNE. At the higher PSNE concentration the focus of heating activity was clearly resolved in all of the experiments and showed a consistent shift towards the FUS transducer which increased over the duration of the sonication on-time. After the end of sonication (50s) the peak temperature began to fall and remained in a fixed location.

3.6. PAM data vs. PSNE concentration

Passive acoustic maps showing the distribution of cavitation energy integrated over each experiment as a function of PSNE concentration are show in Figure 7a. The presence of the PSNE resulted in an increase in the amplitude of acoustic emissions compared to control gels without PSNE, which appeared close to the geometric focus of the FUS transducer in the PAM images. In the control experiments and those at the lowest concentrations of PSNE, cavitation did not occur in all of the experiments, so the mean amplitude of acoustic emissions was not significantly above the background electrical noise and location estimates are not meaningful. As the concentration of PSNE was increased the amplitude of emissions increased and shifted prefocally towards the FUS transducer. At the highest PSNE concentration the location of activity became increasingly prefocal but was more spread out, leading to lower peak value. These effects were maintained over three trials in new gels per condition (Figure 7b–c).

3.7. MRI thermometry vs. PSNE concentration

MRI thermometry images showing focal heating as a function of PSNE concentration are show in Figure 8a. Using PSNE at low concentrations had no significant effect on the location or amplitude of temperature rise compared to the control gels without PSNE. As the concentration of PSNE was increased the amplitude of heating increased and shifted prefocally towards the FUS transducer in a similar manner to the PAM data described above. These effects were maintained over three trials per condition (Figure 8b–c).

3.8. Correlation between PAM and MRI data

The correlation between the PAM and MRI data is shown in Figure 9. The amplitude metrics (maximum cavitation power from PAM vs. maximum temperature rise from MRI, Figure 9a) were well correlated over the full data set (ρ=0.83, $p<0.0001$) with an approximately linear relationship. This confirmed that cavitation-enhanced heating took place, and that the magnitude of the effect scaled with PSNE concentration as expected.

The location metrics (peak location in the FUS propagation direction; Figure 9b) were analyzed as two sub-groups based upon the PSNE concentration, since this would indicate the likelihood of cavitation-enhanced heating. In the control experiments and gels with 2% PSNE (Figure 9b(i)), cavitation was not sufficient in amplitude to result in significant heating enhancement. The location of the peak in MRI was thus essentially unaffected, and

varied between repeats by only a few voxels within the MRI scan resolution. The location of the peak value in the acoustic maps was either close to focal point (in the runs in which cavitation occurred) or not meaningful (e.g. from background electrical noise) in runs without cavitation. As such, the location of activity in the PAM and MRI data were not significantly correlated (ρ=0.51, p>0.05) under these conditions. The experiments that used 5% or higher concentration of PSNE (Figure 9b(i)) showed a good correlation between the location of the focus observed using PAM and MRI (ρ=0.93, p<0.0001) due to cavitation enhanced heating. While the relationship between the two was linear it should be noted that the magnitude of the shift observed with MRI was consistently larger than the PAM data (see discussion).

4. Discussion

In this study the ability of phase-shift nanoemulsions to promote cavitation and hence enhance heating was evaluated using simultaneous passive acoustic mapping and MRI thermometry in a tissue phantom model within the bore of a clinical MRI scanner.

PSNE were produced with a narrow size distribution close to the 200 nm pore size of the membrane used to produce them, similar to previous work (Burgess and Porter 2015, Kopechek *et al* 2014). Microscope images pre- and post-sonication (Figure 2) confirmed large particles were not present initially in the sample and that PSNE could be vaporized into microbubbles. It should be noted that the microbubbles observed in solution in this study were probably larger than would occur from PSNE embedded in hydrogels (or indeed tissue) due to the free motion of particles making coalescence more likely, as well as the use of a low frequency sonicator probe (Brotchie *et al.* 2009).

Pressure ramp experiments (Figure 3) showed that sonication above the vaporization threshold resulted in a significant increase in acoustic emissions compared to gels without PSNE. This suggests that the embedded PSNE were successfully vaporized and in doing so were able to promote cavitation. As the driving pressure was increased the frequency spectra of the acoustic emissions followed the familiar progression typically observed from acoustic cavitation: harmonics, followed by ultraharmonics and finally broadband noise (Leighton 1994). This is qualitatively similar to that reported with microbubbles in previous work (Crake *et al* 2016, 2015). A direct comparison to microbubbles may be of interest for future work but was not attempted here as the limited stability of microbubbles is incompatible with the hydrogel model.

B-mode images interspersed between sonication pulses (Figure 4) showed formation of a bubble cloud in PSNE-containing tissue phantoms due to vaporization of the emulsion into microbubbles. Overlaying co-registered passive acoustic maps produced from the acoustic emissions *during* sonication showed the focus of acoustic emissions coincided with the center of the observed bubble cloud. After sonication ceased the bubble cloud rapidly dissolved and was no longer visible in B-mode images. It should be noted that a bubble cloud was not visible in every B-mode image, even when cavitation was shown to occur in the passive data. There are two main reasons for this. First, as B-mode imaging requires time for round-trip propagation and cannot be conducted simultaneous with therapeutic pulses

this introduces an unavoidable delay compared to the passive images, which could allow for bubble cloud dissolution (Maxwell *et al* 2011). Second, as B-mode is an active modality in order for a bubble cloud to appear it must be sufficiently large and echogenic to reflect the transmitted wavefront, while passive imaging is based upon the emissions inherently generated by cavitation, so could in principle detect the emissions from even a single bubble. Here, the addition of PAM shows that the bubble cloud observed from vaporized PSNE (Kopechek *et al* 2012) can indeed promote cavitation, and that the focus of the resulting activity coincides with the center of the bubble cloud.

The progression of passive acoustic maps and MRI thermometry over time were evaluated for three different experimental conditions: no PSNE (control), low concentration of PSNE (5%) and high concentration PSNE (20%), to evaluate the effect of PSNE-induced cavitation at both ‘sub-thermal’ amplitudes as well as at higher cavitation power which was more likely to result in enhanced heating. The evolution of passive acoustic maps over time (Figure 5) illustrated a lack of significant cavitation activity in the control experiments, which was increased 60–100 fold in presence of PSNE. As the concentration of PSNE was increased the proportion of the sonication over which cavitation occurred also increased, leading to an increase in the total energy of the acoustic emissions. Over time, particularly at the higher PSNE concentration, the position of the focus of cavitation activity was observed to shift towards the FUS transducer. This may be due to several factors including increased absorption of the incoming wave due to formation of a bubble cloud, in addition to secondary stimulation of vaporization due to the broadband acoustic emissions from the cavitating bubbles themselves and/or increased temperature. Prefocal growth of lesions generated by vaporized nanoemulsions has previously been observed optically (Zhang *et al* 2013) however to the best of our knowledge this work represents the first observation of them utilizing acoustic mapping. To evaluate how the PSNE-induced focal cavitation might affect the progression of temperature rise we subsequently examined MRI thermometry data gathered during the same set of experiments.

The progression of MRI thermometry data over time (Figure 6) showed broadly similar trends to the acoustic data in that the addition of PSNE resulted in greater amplitude of activity (temperature rise) as well as a gradual shift in the location of activity towards the FUS transducer as sonication continued. Notably, while at the lower PSNE concentration (5%) the PAM data suggested the presence of some (sporadic and/or low amplitude) cavitation activity, it was insufficient to significantly affect the maximum temperature rise or its location. By contrast, when the PSNE concentration was increased the temperature rise rapidly increased to approximately double that of the control experiments, while the location of peak heating began to shift towards the FUS transducer. Since the precise concentration of accumulated PSNE in tissue is unlikely to be known *in vivo*, comparison of the PAM and MRI data for these experiments provides an illustration of the relative strengths and weaknesses of the methods. While the MRI thermometry data is more readily quantitative, the PAM data has higher frame rate and sensitivity (i.e. the effect of highly diluted PSNE was evident in the PAM data, but not in MRI). Real time PAM could thus be used to predict the likelihood of cavitation-enhanced heating before this would be visible on MRI.

Passive acoustic maps generated from sonications at different PSNE concentrations (Figure 7) showed that the amplitude of acoustic emissions increased with PSNE concentration. As the PSNE concentration was increased the size of the focal region shown in the maps was also observed to increase. This is expected due to the higher density of cavitation nuclei. The location of activity was also observed to shift towards the FUS transducer (i.e. became increasingly prefocal) with PSNE concentration. At the highest PSNE concentration tested, the location of cavitation was closest to the FUS transducer, however the spatial distribution of activity was more diffuse with a lower peak energy than more dilute PSNE samples. These results suggest the formation of a large bubble cloud and possible shielding effects. Such an effect may be beneficial in some scenarios in which treatment over a large area is desirable, but high intensities of cavitation are not necessarily required (e.g. cavitation-enhanced drug delivery to a tumor). However, this effect is likely to be detrimental for purely thermal therapies such as that explored here. It remains to be established whether a concentration of PSNE so high as to result in shielding would be reached via accumulation through leaky vasculature *in vivo*.

MRI thermometry of sonications at different PSNE concentrations (Figure 8) showed similar trends to the PAM data but with a threshold effect. At low concentrations of PSNE the location and amplitude of heating were similar to those observed in control gels, and maximum temperature rise (~10°C) would be insufficient to result in lesions *in vivo*. As the PSNE concentration was increased the temperature rise approximately doubled, reaching the range required to produce thermal lesions (McDannold *et al.* 2000). The location of activity moved towards the FUS transducer in a similar manner to the PAM data discussed above, suggesting that the increase in temperature was as a result of cavitation-enhanced heating.

Comparison of the PAM and MRI data over the full data set (Figure 9) showed a linear correlation between the amplitude of acoustic emissions and the resulting temperature rise. These results confirmed that cavitation-enhanced heating took place, and that the magnitude of the heating enhancement scaled with PSNE concentration as expected. In the cases where cavitation occurred the focus of activity was also well correlated between the two methods, however the magnitude of the shift in location of focal heating was consistently larger than that of the cavitation activity. This observation is likely a combination of two factors. First, as ultrasound was delivered from one side of the phantom, it is possible that absorption and/or shielding effects could result in a bias in which heating is increased on the side of the bubble cloud closest to the FUS transducer. In clinical practice, using large aperture (e.g. hemispherical) transducers, this effect is likely to be reduced as the incoming ultrasound arrives over a larger range of angles. Second, the metrics used here were based upon PAM data summed over time, which could result in spatial averaging towards the average position of cavitation activity. Alternative PAM metrics based upon the observations here (e.g. utilizing a threshold and sum, or thermal modeling (Jensen *et al* 2013)) may be more appropriate for comparison to the peak temperature maps and could be explored in future work. Nonetheless, the two methods remained well correlated over the conditions explored here, which suggests that the degree in heating and/or observation bias scaled with the magnitude of cavitation activity and PSNE concentration.

The study as presented has several limitations which could be explored in future work. First, with regards to the acoustic setup, due to the use of a linear array it was not possible to observe the full three-dimensional distribution of cavitation activity, resulting in a lack of information in the elevational direction. In addition the PAM data appeared elongated in the axial direction of the array due to the point spread function. The use of a larger aperture 2D array could resolve these issues in future studies. Second, the MRI thermometry data were also acquired in a single plane, so could not predict heating in three dimensions and may be affected by averaging over the slice thickness. While similar single-plane sequences are used clinically, the use of a 3D imaging sequence may provide more spatial information at the possible expense of SNR and/or frame rate. Third, the metrics used to analyze the PAM and MRI data were relatively basic and could be improved in future work, for example by calculating thermal center of mass instead of the simple peak location. Finally, while this study explored the relationship between acoustic activity and heating, the ultimate goal of such a therapy is to produce lesions. In this study we did observe changes in the PSNE-containing phantoms in T2-weighted MRI acquired after sonication; however such a sequence is too slow for use during sonication. These “lesions” could also be observed optically after the sonications, but real-time visualization was not practical here due to the constraints of space, water and MR-compatibility within the scanner bore. On a more fundamental level, the relationship between heating and lesioning (and propensity of cavitation to promote them) have been extensively studied, and reliance on lesioning risks introduction of secondary effects (e.g. variable response to temperature between samples or tissue types) which could obscure the underlying mechanism, while the novelty here is in the simultaneous spatiotemporal monitoring of both cavitation activity and the resulting temperature rise produced by embedded nanoemulsions. Nonetheless, examination of the correlation between observed thermally-induced changes and maps of cavitation and/or heating would be worthwhile for future studies, for example by incorporating passive acoustic mapping alongside optical monitoring (Zhang *et al* 2013), optimization of the MR sequence to permit more rapid imaging using a sequence which is sensitive to lesions, and/or development of an MR-compatible means of optical lesion detection.

5. Conclusions

Phase-shift nanoemulsions were produced and employed to enhance acoustic cavitation and temperature rise in an *in vitro* model. Under simultaneous passive acoustic imaging and magnetic resonance thermometry the nanoemulsions were shown to result in focal cavitation and heating which translated towards the driving focused ultrasound transducer over time. The magnitude of the increase in cavitation and focal shift both scaled with nanoemulsion concentration. Passive acoustic mapping results were well correlated with MRI thermometry and had greater sensitivity. These results show that phase-shift nanoemulsions could be beneficial for enhancement of thermal focused ultrasound therapies and that passive acoustic mapping could be beneficial for monitoring of this process.

Acknowledgments

The authors would like to acknowledge NIH for supporting this work (grant number R01EB016102), Christian Coviello for assistance with the robust Capon beamformer algorithm, and Costas Arvanitis, Jason White and Spencer Brinker for helpful discussions.

References

Albrecht T, Blomley M, Bolondi L, Claudon M, Correas J-M, Cosgrove D, Greiner L, Jäger K, de Jong N, Leen E, Lencioni R, Lindsell D, Martegani A, Solbiati L, Thorelius L, Tranquart F, Weskott HP, Whittingham T. Guidelines for the Use of Contrast Agents in Ultrasound - January 2004. Ultraschall Med. 2004; 25:249–56. [PubMed: 15300497]

Arvanitis, C., Crake, C., McDannold, N., Clement, G. Passive acoustic mapping with the angular spectrum method. IEEE Transactions on Medical Imaging. 2016. [epub ahead of print] Online: http://ieeexplore.ieee.org/document/7792747/

Arvanitis CD, Livingstone MS, McDannold N. Combined ultrasound and MR imaging to guide focused ultrasound therapies in the brain. Phys Med Biol. 2013; 58:4749–61. [PubMed: 23788054]

Brotchie A, Grieser F, Ashokkumar M. Effect of power and frequency on bubble-size distributions in acoustic cavitation. Physical review letters. 2009; 102:084302. [PubMed: 19257742]

Burgess MT, Porter TM. Acoustic cavitation-mediated delivery of small interfering ribonucleic acids with phase-shift nanoemulsions. Ultrasound Med Biol. 2015; 41:2191–201. [PubMed: 25979417]

Catane R, Beck A, Inbar Y, Rabin T, Shabshin N, Hengst S, Pfeffer RM, Hanannel A, Dogadkin O, Liberman B, Kopelman D. MR-guided focused ultrasound surgery (MRgFUS) for the palliation of pain in patients with bone metastases--preliminary clinical experience. Ann Oncol Off J Eur Soc Med Oncol ESMO. 2007; 18:163–7.

Chen L, ter Haar G, Hill CR, Dworkin M, Carnochan P, Young H, Bensted JPM. Effect of blood perfusion on the ablation of liver parenchyma with high-intensity focused ultrasound. Phys Med Biol. 1993; 38:1661. [PubMed: 8272440]

Choi JJ, Coussios C-C. Spatiotemporal evolution of cavitation dynamics exhibited by flowing microbubbles during ultrasound exposure. J Acoust Soc Am. 2012; 132:3538–49. [PubMed: 23145633]

Chung AH, Hynynen K, Colucci V, Oshio K, Cline HE, Jolesz FA. Optimization of spoiled gradient-echo phase imaging for in vivo localization of a focused ultrasound beam. Magn Reson Med. 1996; 36:745–52. [PubMed: 8916025]

Claudon M, Dietrich C, Choi B, Cosgrove D, Kudo M, Nolsøe C, Piscaglia F, Wilson S, Barr R, Chammas M, Chaubal N, Chen M-H, Clevert D, Correas J, Ding H, Forsberg F, Fowlkes J, Gibson R, Goldberg B, Lassau N, Leen E, Mattrey R, Moriyasu F, Solbiati L, Weskott H-P, Xu H-X. Guidelines and Good Clinical Practice Recommendations for Contrast Enhanced Ultrasound (CEUS) in the Liver – Update 2012. Ultraschall Med - Eur J Ultrasound. 2012; 34:11–29.

Coussios C-C, Farny CH, ter Haar G, Roy RA. Role of acoustic cavitation in the delivery and monitoring of cancer treatment by high-intensity focused ultrasound (HIFU). Int J Hyperthermia. 2007; 23:105–20. [PubMed: 17578336]

Coviello C, Kozick R, Choi J, Gyöngy M, Jensen C, Smith PP, Coussios C-C. Passive acoustic mapping utilizing optimal beamforming in ultrasound therapy monitoring. J Acoust Soc Am. 2015; 137:2573–85. [PubMed: 25994690]

Crake C, Owen J, Smart S, Coviello C, Coussios C-C, Carlisle R, Stride E. Enhancement and Passive Acoustic Mapping of Cavitation from Fluorescently Tagged Magnetic Resonance-Visible Magnetic Microbubbles In Vivo. Ultrasound Med Biol. 2016; 42:3022–3036. [PubMed: 27666788]

Crake C, de Saint Victor M, Owen J, Coviello C, Collin J, Coussios C-C, Stride E. Passive acoustic mapping of magnetic microbubbles for cavitation enhancement and localization. Phys Med Biol. 2015; 60:785–806. [PubMed: 25564961]

Dayton PA, Zhao S, Bloch SH, Schumann P, Penrose K, Matsunaga TO, Zutshi R, Doinikov A, Ferrara KW. Application of ultrasound to selectively localize nanodroplets for targeted imaging and therapy. Mol Imaging. 2006; 5:7290–2006.

Deng L, O'Reilly MA, Jones RM, An R, Hynynen K. A multi-frequency sparse hemispherical ultrasound phased array for microbubble-mediated transcranial therapy and simultaneous cavitation mapping. Phys Med Biol. 2016; 61:8476. [PubMed: 27845920]

Elias WJ, Lipsman N, Ondo WG, Ghanouni P, Kim YG, Lee W, Schwartz M, Hynynen K, Lozano AM, Shah BB, Huss D, Dallapiazza RF, Gwinn R, Witt J, Ro S, Eisenberg HM, Fishman PS,

Gandhi D, Halpern CH, Chuang R, Butts Pauly K, Tierney TS, Hayes MT, Cosgrove GR, Yamaguchi T, Abe K, Taira T, Chang JW. A Randomized Trial of Focused Ultrasound Thalamotomy for Essential Tremor. N Engl J Med. 2016; 375:730–9. [PubMed: 27557301]

Farny, CH. Identifying and monitoring the roles of cavitation in heating from high-intensity focused ultrasound. PhD Dissertation. 2007. Online: http://open.bu.edu/handle/2144/1377

Farny CH, Holt RG, Roy RA. Temporal and Spatial Detection of HIFU-Induced Inertial and Hot-Vapor Cavitation with a Diagnostic Ultrasound System. Ultrasound Med Biol. 2009; 35:603–15. [PubMed: 19110368]

Gateau J, Aubry J-F, Chauvet D, Boch A-L, Fink M, Tanter M. In vivo bubble nucleation probability in sheep brain tissue. Phys Med Biol. 2011a; 56:7001–15. [PubMed: 22015981]

Gateau J, Aubry J-F, Pernot M, Fink M, Tanter M. Combined passive detection and ultrafast active imaging of cavitation events induced by short pulses of high-intensity ultrasound. IEEE Trans Ultrason Ferroelectr Freq Control. 2011b; 58:517–32. [PubMed: 21429844]

Gyöngy, M. DPhil Thesis. University of Oxford; 2010. Passive Cavitation Mapping for Monitoring Ultrasound Therapy. Online: http://ora.ox.ac.uk/objects/uuid:af6f3c5a-bec5-4378-a617-c89d2b16d95d

Gyongy M, Coussios C-C. Passive Spatial Mapping of Inertial Cavitation During HIFU Exposure. IEEE Trans Biomed Eng. 2010; 57:48–56. [PubMed: 19628450]

ter Haar G, Sinnett D, Rivens I. High intensity focused ultrasound-a surgical technique for the treatment of discrete liver tumours. Phys Med Biol. 1989; 34:1743. [PubMed: 2685839]

Hall TJ, Bilgen M, Insana MF, Krouskop TA. Phantom materials for elastography. IEEE Trans Ultrason Ferroelectr Freq Control. 1997; 44:1355–65.

Haworth KJ, Mast TD, Radhakrishnan K, Burgess MT, Kopechek JA, Huang S-L, McPherson DD, Holland CK. Passive imaging with pulsed ultrasound insonations. J Acoust Soc Am. 2012; 132:544–53. [PubMed: 22779500]

Heppner GH, Miller BE. Tumor heterogeneity: biological implications and therapeutic consequences. Cancer and Metastasis Reviews. 1983; 2:5–23. [PubMed: 6616442]

Holt RG, Roy RA. Measurements of bubble-enhanced heating from focused, mhz-frequency ultrasound in a tissue-mimicking material. Ultrasound Med Biol. 2001; 27:1399–412. [PubMed: 11731053]

Hynynen K. The threshold for thermally significant cavitation in dog's thigh muscle in vivo. Ultrasound Med Biol. 1991; 17:157–169. [PubMed: 2053212]

Hynynen K, Pomeroy O, Smith DN, Huber PE, McDannold NJ, Kettenbach J, Baum J, Singer S, Jolesz FA. MR Imaging-guided Focused Ultrasound Surgery of Fibroadenomas in the Breast: A Feasibility Study. Radiology. 2001; 219:176–85. [PubMed: 11274554]

Illing RO, Kennedy JE, Wu F, ter Haar GR, Protheroe AS, Friend PJ, Gleeson FV, Cranston DW, Phillips RR, Middleton MR. The safety and feasibility of extracorporeal high-intensity focused ultrasound (HIFU) for the treatment of liver and kidney tumours in a Western population. Br J Cancer. 2005; 93:890–5. [PubMed: 16189519]

Ishida O, Maruyama K, Sasaki K, Iwatsuru M. Size-dependent extravasation and interstitial localization of polyethyleneglycol liposomes in solid tumor-bearing mice. Int J Pharm. 1999; 190:49–56. [PubMed: 10528096]

Ishihara Y, Calderon A, Watanabe H, Okamoto K, Suzuki Y, Kuroda K. A precise and fast temperature mapping using water proton chemical shift. Magn Reson Med. 1995; 34:814–23. [PubMed: 8598808]

Jensen CR, Cleveland RO, Coussios CC. Real-time temperature estimation and monitoring of HIFU ablation through a combined modeling and passive acoustic mapping approach. Phys Med Biol. 2013; 58:5833–50. [PubMed: 23920089]

Jensen CR, Ritchie RW, Gyöngy M, Collin T JR, Leslie T, Coussios C-C. Spatiotemporal Monitoring of High-Intensity Focused Ultrasound Therapy with Passive Acoustic Mapping. Radiology. 2012; 262:252–61. [PubMed: 22025731]

Jolesz FA. MRI-guided focused ultrasound surgery. Annu Rev Med. 2009; 60:417–30. [PubMed: 19630579]

Kennedy JE. High-intensity focused ultrasound in the treatment of solid tumours. Nat Rev Cancer. 2005; 5:321–327. [PubMed: 15776004]

Kopechek JA, Park E, Mei C-S, McDannold NJ, Porter TM. Accumulation of phase-shift nanoemulsions to enhance MR-guided ultrasound-mediated tumor ablation in vivo. J Healthc Eng. 2013; 4:109–126. [PubMed: 23502252]

Kopechek JA, Park E-J, Zhang Y-Z, Vykhodtseva NI, McDannold NJ, Porter TM. Cavitation-enhanced MR-guided focused ultrasound ablation of rabbit tumors *in vivo* using phase shift nanoemulsions. Phys Med Biol. 2014; 59:3465–81. [PubMed: 24899634]

Kopechek JA, Zhang P, Burgess MT, Porter TM. Synthesis of Phase-shift Nanoemulsions with Narrow Size Distributions for Acoustic Droplet Vaporization and Bubble-enhanced Ultrasound-mediated Ablation. J Vis Exp JoVE. 2012; 67:e4308.

Kripfgans OD, Fabiilli ML, Carson PL, Fowlkes JB. On the acoustic vaporization of micrometer-sized droplets. J Acoust Soc Am. 2004; 116:272–81. [PubMed: 15295987]

Kripfgans OD, Fowlkes JB, Miller DL, Eldevik OP, Carson PL. Acoustic droplet vaporization for therapeutic and diagnostic applications. Ultrasound Med Biol. 2000; 26:1177–89. [PubMed: 11053753]

Lafon C, Zderic V, Noble ML, Yuen JC, Kaczkowski PJ, Sapozhnikov OA, Chavrier F, Crum LA, Vaezy S. Gel phantom for use in high-intensity focused ultrasound dosimetry. Ultrasound Med Biol. 2005; 31:1383–9. [PubMed: 16223642]

Lee JY, Carugo D, Crake C, Owen J, de Saint Victor M, Seth A, Coussios C, Stride E. Nanoparticle-Loaded Protein–Polymer Nanodroplets for Improved Stability and Conversion Efficiency in Ultrasound Imaging and Drug Delivery. Adv Mater. 2015; 27:5484–5492. [PubMed: 26265592]

Leighton, TG. The Acoustic Bubble. London: Academic Press; 1994.

Lele, PP. Ultrasound. Springer; 1987. Effects of ultrasound on “solid” mammalian tissues and tumors in vivo; p. 275-306.Online: http://link.springer.com/chapter/10.1007/978-1-4613-1811-8_21

Leslie TA, Kennedy JE, Illing RO, Ter Haar GR, Wu F, Phillips RR, Friend PJ, Roberts ISD, Cranston DW, Middleton MR. High-intensity focused ultrasound ablation of liver tumours: can radiological assessment predict the histological response? Br J Radiol. 2008; 81:564– 71. [PubMed: 18559903]

Maeda H, Wu J, Sawa T, Matsumura Y, Hori K. Tumor vascular permeability and the EPR effect in macromolecular therapeutics: a review. J Controlled Release. 2000; 65:271–84.

Maxwell AD, Wang TY, Cain CA, Fowlkes JB, Sapozhnikov OA, Bailey MR, Xu Z. Cavitation clouds created by shock scattering from bubbles during histotripsy. J Acoust Soc Am. 2011; 130:1888–1898. [PubMed: 21973343]

McDannold NJ, King RL, Jolesz FA, Hynynen KH. Usefulness of MR Imaging-Derived Thermometry and Dosimetry in Determining the Threshold for Tissue Damage Induced by Thermal Surgery in Rabbits. Radiology. 2000; 216:517–23. [PubMed: 10924580]

McDannold NJ, Vykhodtseva NI, Hynynen K. Microbubble contrast agent with focused ultrasound to create brain lesions at low power levels: MR imaging and histologic study in rabbits. Radiology. 2006; 241:95–106. [PubMed: 16990673]

Mougenot C, Salomir R, Palussière J, Grenier N, Moonen CTW. Automatic spatial and temporal temperature control for MR-guided focused ultrasound using fast 3D MR thermometry and multispiral trajectory of the focal point. Magn Reson Med. 2004; 52:1005–15. [PubMed: 15508173]

Myers R, Coviello C, Erbs P, Foloppe J, Rowe C, Kwan J, Crake C, Finn S, Jackson E, Balloul J-M, et al. Polymeric Cups for Cavitation-mediated Delivery of Oncolytic Vaccinia Virus. Mol Ther. 2016 [Epub ahead of print].

O’Reilly MA, Jones RM, Hynynen K. Three-Dimensional Transcranial Ultrasound Imaging of Microbubble Clouds Using a Sparse Hemispherical Array. Biomed Eng IEEE Trans On. 2014; 61:1285–94.

Palussière J, Salomir R, Le Bail B, Fawaz R, Quesson B, Grenier N, Moonen CTW. Feasibility of MR-guided focused ultrasound with real-time temperature mapping and continuous sonication for ablation of VX2 carcinoma in rabbit thigh. Magn Reson Med Off J Soc Magn Reson Med Soc Magn Reson Med. 2003; 49:89–98.

Peters RTD, Hinks RS, Henkelman RM. Ex vivo tissue-type independence in proton-resonance frequency shift MR thermometry. Magn Reson Med. 1998; 40:454–9. [PubMed: 9727949]

Quesson B, de Zwart JA, Moonen CT. Magnetic resonance temperature imaging for guidance of thermotherapy. J Magn Reson Imaging. 2000; 12:525–533. [PubMed: 11042633]

Reznik N, Seo M, Williams R, Bolewska-Pedyczak E, Lee M, Matsuura N, Gariepy J, Foster FS, Burns PN. Optical studies of vaporization and stability of fluorescently labelled perfluorocarbon droplets. Phys Med Biol. 2012; 57:7205. [PubMed: 23060210]

Salgaonkar VA, Datta S, Holland CK, Mast TD. Passive cavitation imaging with ultrasound arrays. J Acoust Soc Am. 2009; 126:3071. [PubMed: 20000921]

Sokka SD, King R, Hynynen K. MRI-guided gas bubble enhanced ultrasound heating in in vivo rabbit thigh. Phys Med Biol. 2003; 48:223. [PubMed: 12587906]

Stewart EA, Gedroyc WMW, Tempany CMC, Quade BJ, Inbar Y, Ehrenstein T, Shushan A, Hindley JT, Goldin RD, David M, Sklair M, Rabinovici J. Focused ultrasound treatment of uterine fibroid tumors: safety and feasibility of a noninvasive thermoablative technique. Am J Obstet Gynecol. 2003; 189:48–54. [PubMed: 12861137]

Tempany CMC, Stewart EA, McDannold N, Quade BJ, Jolesz FA, Hynynen K. MR imaging-guided focused ultrasound surgery of uterine leiomyomas: a feasibility study. Radiology. 2003; 226:897–905. [PubMed: 12616023]

Thüroff S, Chaussy C, Vallancien G, Wieland W, Kiel HJ, le Duc A, Desgrandchamps F, de la Rosette JJMCH, Gelet A. High-Intensity Focused Ultrasound and Localized Prostate Cancer: Efficacy Results from the European Multicentric Study. J Endourol. 2003; 17:673–7. [PubMed: 14622488]

Tran BC, Seo J, Hall TL, Fowlkes JB, Cain CA. Microbubble-enhanced cavitation for noninvasive ultrasound surgery. IEEE Trans Ultrason Ferroelectr Freq Control. 2003; 50:1296–1304. [PubMed: 14609069]

Tung Y-S, Liu H-L, Wu C-C, Ju K-C, Chen W-S, Lin W-L. Contrast-agent-enhanced ultrasound thermal ablation. Ultrasound Med Biol. 2006; 32:1103–10. [PubMed: 16829324]

U.S. Food and Drug Administration. Press Announcements - FDA approves first MRI-guided focused ultrasound device to treat essential tremor. 2016. Online: http://www.fda.gov/NewsEvents/Newsroom/PressAnnouncements/ucm510595.htm

U.S. Food and Drug Administration. Recently-Approved Devices - ExAblate® 2000 System - P040003. 2004. Online: http://www.fda.gov/medicaldevices/productsandmedicalprocedures/deviceapprovalsandclearances/recently-approveddevices/ucm080704.htm

Vignon F, Shi WT, Powers JE, Everbach EC, Jinjin L, Shunji G, Feng X, Porter TR. Microbubble cavitation imaging. Ultrason Ferroelectr Freq Control IEEE Trans On. 2013; 60:661–70.

Wang X, Sun J. High-intensity focused ultrasound in patients with late-stage pancreatic carcinoma. Chin Med J (Engl). 2002; 115:1332–5. [PubMed: 12411106]

Wu F, Wang Z-B, Chen W-Z, Zou J-Z, Bai J, Zhu H, Li K-Q, Xie F-L, Jin C-B, Su H-B, Gao G-W. Extracorporeal focused ultrasound surgery for treatment of human solid carcinomas: early Chinese clinical experience. Ultrasound Med Biol. 2004; 30:245–60. [PubMed: 14998677]

Wu F, Wang Z-B, Zhu H, Chen W-Z, Zou J-Z, Bai J, Li K-Q, Jin C-B, Xie F-L, Su H-B. Feasibility of US-guided High-Intensity Focused Ultrasound Treatment in Patients with Advanced Pancreatic Cancer: Initial Experience. Radiology. 2005; 236:1034–40. [PubMed: 16055692]

Yang R, Sanghvi NTM, Rescorla FJ, Galliani CA, Fry FJM, Griffith SL, Grosfeld JL. Extracorporeal Liver Ablation Using Sonography-Guided High-Intensity Focused Ultrasound. Invest Radiol. 1992; 27:796–803. [PubMed: 1399435]

Yu T, Wang G, Hu K, Ma P, Bai J, Wang Z. A microbubble agent improves the therapeutic efficiency of high intensity focused ultrasound: a rabbit kidney study. Urol Res. 2003; 32:14–9. [PubMed: 14655029]

Yuan F, Dellian M, Fukumura D, Leunig M, Berk DA, Torchilin VP, Jain RK. Vascular permeability in a human tumor xenograft: molecular size dependence and cutoff size. Cancer Res. 1995; 55:3752–6. [PubMed: 7641188]

Zhang M, Fabiilli ML, Haworth KJ, Padilla F, Swanson SD, Kripfgans OD, Carson PL, Fowlkes JB. Acoustic Droplet Vaporization for Enhancement of Thermal Ablation by High Intensity Focused Ultrasound. Acad Radiol. 2011; 18:1123–32. [PubMed: 21703883]

Zhang P, Kopechek JA, Porter TM. The impact of vaporized nanoemulsions on ultrasound-mediated ablation. J Ther Ultrasound. 2013:1–2. [PubMed: 24761222]

Zhang P, Porter T. An in vitro Study of a Phase-Shift Nanoemulsion: A Potential Nucleation Agent for Bubble-Enhanced HIFU Tumor Ablation. Ultrasound Med Biol. 2010; 36:1856–66. [PubMed: 20888685]

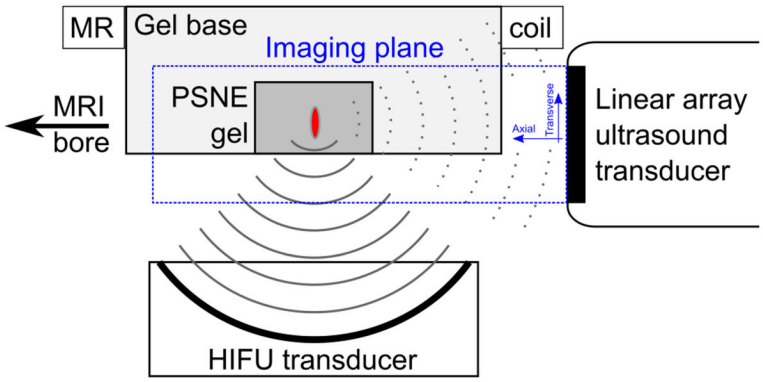

Figure 1.

Experimental setup (not to scale). Polyacrylamide hydrogels with and without PSNE were placed in a sample holder at the focus of a high intensity focused ultrasound (HIFU) transducer. The acoustic emissions were monitored using an ultrasound linear array aligned with the focal point. Transverse and axial directions were defined relative to the center of the front face of the imaging array. The assembly was placed in a tank of degassed deionized water at 37°C and placed within the bore of a 3T clinical MRI scanner.

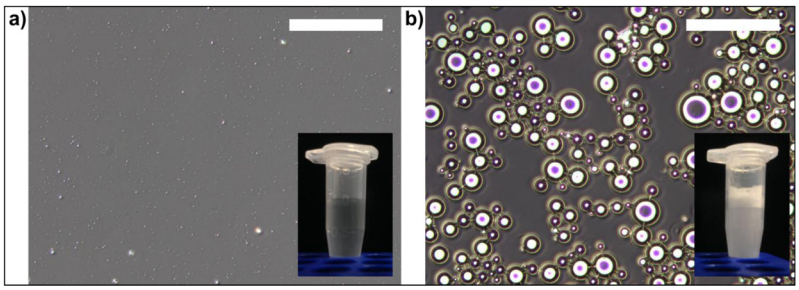

Figure 2.

Phase contrast microscope images (scale bar = 100μm) showing 10% PSNE suspension (a) before and (b) after sonication with the probe sonicator. Inset photographs show macroscopic appearance of the solution.

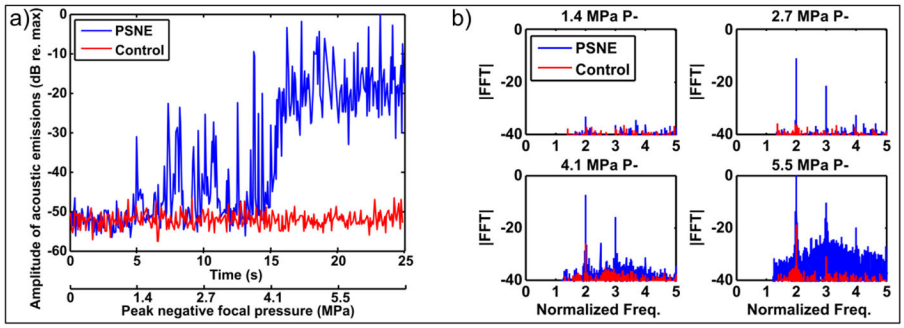

Figure 3.

Cavitation threshold determination. Hydrogels with and without PSNE were sonicated at escalating peak negative focal pressure while the acoustic emissions were recorded using the array. (a) The amplitude of acoustic emissions (indicative of source power) was extracted from the beamformed data. The plot shows 5 seconds of data at each pressure step. (b) Frequency spectra (FFT magnitude) for the 4 pressure steps.

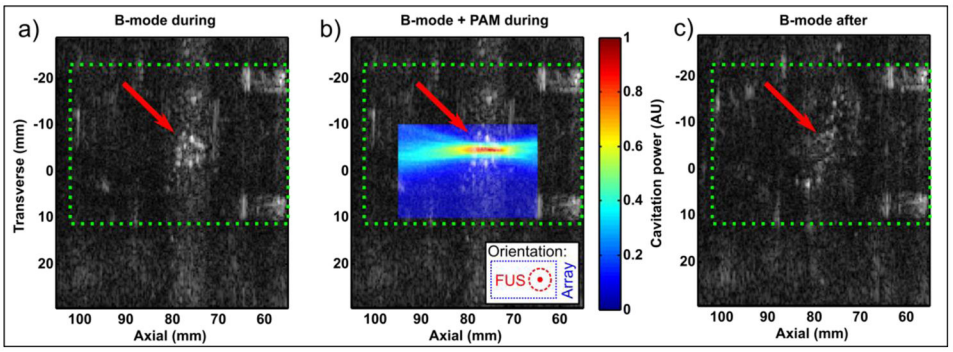

Figure 4.

Monitoring of PSNE vaporization with B-mode and PAM. Green dotted rectangle indicates the outline of the hydrogel, and red arrow the position of the FUS transducer focus. (a) B-mode image taken during sonication showing formation of a bubble cloud (arrow). (b) The same B-mode image with co-registered PAM (passive) image showing cavitation coincident with the bubble cloud. Inset shows orientation with array to right of image and FUS out of page. (c) B-mode image taken after sonication showing dissolution.

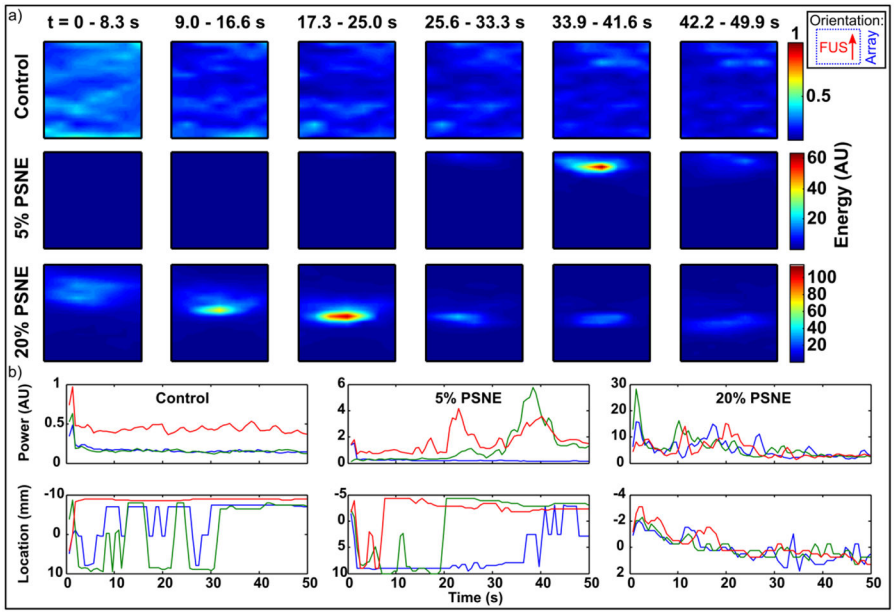

Figure 5.

Evolution of passive acoustic maps over time. (a) Maps showing the sum of cavitation emissions for subsets of bursts over time for sonication of gels without PSNE (control), low (5%) or high (20%) PSNE concentrations. Color scales are normalized to the control data. Maps show a region of interest of ±4mm transverse, 100–120mm axial with respect to the imaging array. Inset shows orientation with array to right of image and FUS propagation from bottom to top. (b) Amplitude and peak location over time for 3 trials of the 3 conditions.

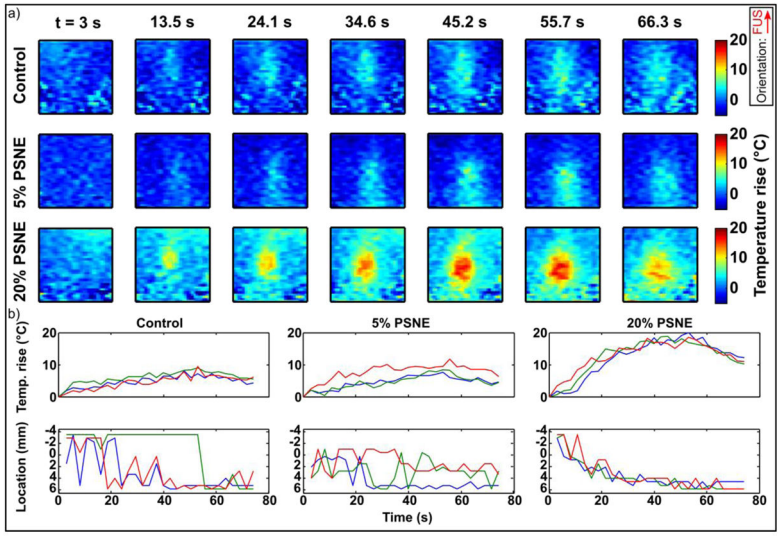

Figure 6.

Evolution of MRI thermometry data over time. (a) Maps of temperature rise over time for sonication of gels without PSNE (control), low (5%) or high (20%) PSNE concentrations. Images show a region of interest of 20 × 20 mm about the focus. Inset shows FUS propagation direction from bottom to top. (b) Peak temperature rise and location over time for 3 trials of the 3 conditions. Note that sonication duration was 50s and monitoring continued for 25s after to capture cooling.

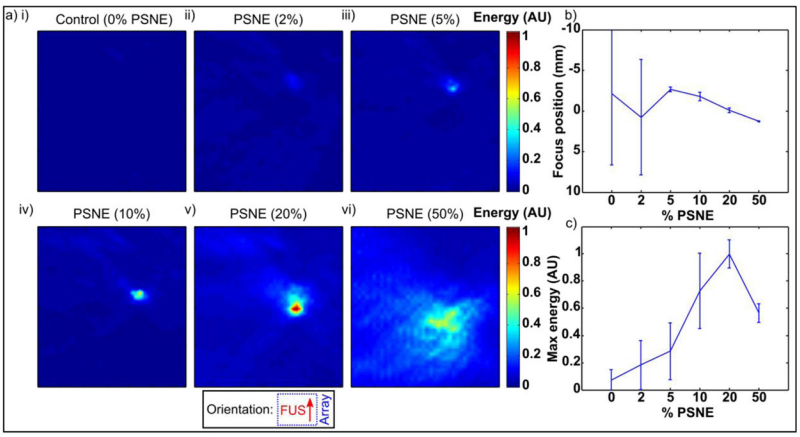

Figure 7.

(a) Passive acoustic maps showing spatial localization of cavitation activity as a function of PSNE concentration. Inset shows orientation with array to right of image and FUS propagation from bottom to top. Maps show a region of interest of ±10mm transverse, 80–200mm axial with respect to the imaging array. Maps show the sum of activity over each experiment. The transverse axis is shown on a finer scale to show detail. (b) Transverse peak location (mm) over 3 trials per condition. (c) Peak energy (AU) over 3 trials per condition.

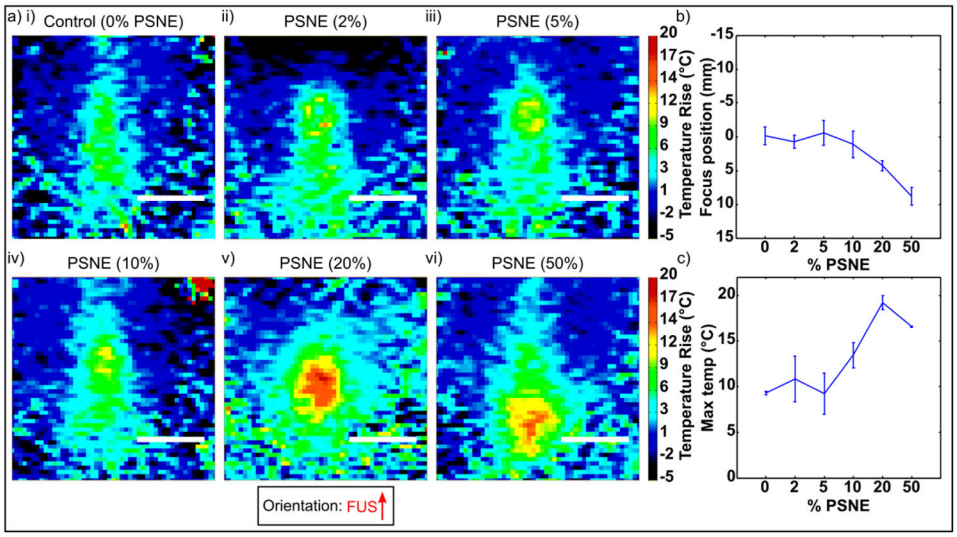

Figure 8.

(a) MRI thermometry showing focal heating as a function of PSNE concentration. Inset shows FUS propagation direction from bottom to top. Maps show temperature rise (baseline 37°C) at the time of maximum temperature in each experiment. Scale bar = 10mm (b) Peak location (mm) in FUS propagation direction over 3 trials per condition. (c) Max temperature rise (°C) over 3 trials per condition.

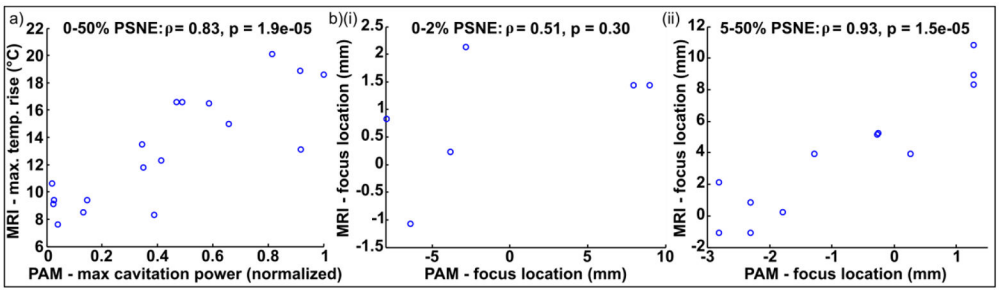

Figure 9.

Correlation between PAM and MRI data. (a) Amplitude: max. cavitation power vs. max. temperature rise. All of the data shown in Figure 7 and 8 is included, with 3 trials for each of the 6 conditions. (b) Location: peak in direction of FUS propagation observed with MRI thermometry vs. PAM. The data was analyzed in two groups based on the PSNE concentration: (i) Control and 2% PSNE (low/zero cavitation); (ii) 5–50% PSNE (cavitation). ρ = Pearson's correlation coefficient, p = statistical significance from t-test.